Natural Hazards (2023) 116:3899–3923
https://doi.org/10.1007/s11069-023-05843-z

ORIGINAL PAPER

Monte Carlo modeling of tornado hazard to wind turbines in Germany

Romane Bouchard[1] · **Djordje Romanic**[1]

Received: 25 October 2022 / Accepted: 29 January 2023 / Published online: 9 February 2023

Abstract
Using a Monte Carlo hazard modeling approach, this study assesses the damage and losses to wind turbines caused by tornadoes over Germany. The model combines observed climatology of tornadoes, exposure map of wind turbines and their capacities, vulnerability curve (first developed in this study), and costs of wind turbines to estimate the likelihood of financial losses of different magnitudes. The losses are presented in terms of aggregated and highest annual losses as a function of the return period. Deterministic modeling of the vulnerability function produced larger variability of the most severe losses (rare, but high-intensity events) compared to the pseudorandom sampling of the damage from the vulnerability curve. Doubling the number of current wind turbines results in smaller expected losses than installing fewer but more powerful units (repowerment). Tornadoes are most frequent in the summer months when the capacity factors of wind farms are the lowest and the electricity consumption is also lower than in the winter months. By repeatedly placing a tornado track of a fixed size over the same wind farm, we further investigated the sensitivity of our model to different parameters. The probability of tornadoes of different intensities hitting a wind turbine over Germany is also calculated.

Keywords Monte Carlo model · Tornado · Wind turbine · Vulnerability · Hazard modeling · Wind energy

1 Introduction

Renewables have been the fastest growing energy sources in European Union, with 80% of new capacities being based on renewable energy (IEA 2017). Specifically, wind energy is expected to become the main source of electricity in the 2030s due to increasing onshore

Romane Bouchard and Djordje Romanic have contributed equally.

✉ Djordje Romanic
djordje.romanic@mcgill.ca

Romane Bouchard
romane.bouchard@mail.mcgill.ca

[1] Department of Atmospheric and Oceanic Sciences, McGill University, 805 Sherbrooke Street West, Montreal, Quebec H3A 0B9, Canada

and offshore installations across Europe. The growth of renewable sources of energy such as wind was not halted even during 2020 when the economies were severely affected by COVID-19 lockdowns (IEA 2021). Because the energy sector contributes to approximately three-quarters of the greenhouse gas emissions (IEA 2021), further investments into renewables in terms of new technologies, policy adaptations, diversification of energy sources, cost of production, as well as reliability of energy supplies are expected to continue. A changing climate, however, also possesses increasing risks of physical damage to wind turbines caused by severe winds and other weather perils. For example, IEA (2021) reported they "...estimate that around a quarter of the world's electricity networks face a high risk of destructive cyclone winds."

Germany is the leading wind energy market in Europe with over 63 GW of total capacity (GTAI 2022) and over 135,000 people working in this sector. In 2021, wind energy accounted for 23% of net German electricity production. Investments in the wind energy sector and favorable policies for wind power generation are only expected to increase moving forward. The country is planning to accelerate the construction of both onshore and offshore wind turbines at new sites. For instance, Germany is aiming to nearly double (to 100 GW) onshore wind power installations by 2030. This goal is in accordance with the aim of a 100% renewable-based energy system by 2050 (Maruf 2021). Wind energy is expected to be the key contributor to achieving this ambitious goal. Therefore, the undisturbed operation of wind farms that are regularly exposed to severe weather conditions is an important factor to consider in this process.

In addition to the increased frequency of cyclones that can be hazardous to wind turbines (IEA 2021), climatological research has indicated that the occurrence of convective environments prone to severe thunderstorms associated with tornadoes is also likely to increase around the world (Diffenbaugh et al. 2013; Allen et al. 2014; Seeley and Romps 2015; Tippett et al. 2015). Together with Bosnia and Herzegovina and France, Germany has the highest frequency of environments favorable for significant tornadoes (Brooks et al. 2003). Lepore et al. (2021) reported an increase in the frequency of proxies of severe weather for between 5% and 20% per °C of global temperature increase. They expect a significant rise in severe weather activity across Europe in the period March–November, which is also the peak tornado season for most of Europe, including Germany (Dotzek 2001).

Tornado activity in Germany is highest in August and lowest in November-March. These monthly variations are driven by the annual trend of thunderstorm activity in this region (Hagen and Finke 1999). Dotzek (2001) found that Germany received between 4 and 7 tornadoes annually with the strongest twister being the Pforzheim F4-rated tornado in July 1968. Here, Fujita (F) scale (Fujita 1971) is used as a discrete measure of tornado damage intensity with the strongest tornadoes (F5) being associated with "incredible damage" (wind speeds over 112 m s^{-1}) and F0 being the weakest tornadoes causing "light damage" (wind speeds between 18 and 32 m s^{-1}). However, Dotzek (2001) also reported that the actual number of tornadoes in Germany is probably around 4 times higher than the above figure that is based on official tornado reports. Hence, Dotzek (2001) concluded his study with the following statement: "*Only by mere chance, tornadoes have not yet caused many fatalities in Germany, and their damage potential is therefore still underestimated*." Indeed, more recent studies show that Germany has the highest density of reported tornadoes across Europe (Groenemeijer and Kühne 2014) with an overall decrease in tornado occurrence from the northwest to the southeast of the country. The increasing number of installed wind turbines provides additional exposure to potentially harmful effects of tornadoes on these structures (Romanic et al. 2018).

All considered—namely, Germany's high annual number of tornadoes and the largest wind energy sector in Europe—this study assesses the physical damage and associated financial losses that tornadoes might inflict on onshore wind farms across Germany. The present study is based on a hazard and risk modeling approach using Monte Carlo simulations, similar to Romanic et al. (2016), Refan et al. (2020), Strader et al. (2016), Arnold and Yildiz (2015), Sarajcev et al. (2013), Daneshvaran and Morden (2007), to name a few. While these types of models have been operationally used for over a decade in the private insurance sector, most of them have not been published and their methodology is still undisclosed. Therefore, they are of limited, if any, use to researchers, the public sector, wind farm developers and operators, as well as decision-makers outside of the insurance industry. This study combines the observed climatology of tornadoes over Germany with the exposure map of wind turbines and vulnerability curves, which quantify the damage that tornadoes of different strengths inflict on wind turbines, to assess potential risks and losses due to damage caused by tornadoes to wind turbines.

This paper is organized in the following manner. Section 2 describes the methodology that was used to develop our hazard model. Section 3 presents the results in the form of exceedance curves and modeled spatial occurrence of tornadoes over the wind turbine exposure map of Germany. We also address the risks associated with the projected increase of installed wind capacities by (1) increasing the number of units twofold while following a similar capacity apportioning as the currently installed wind turbines; and (2) repowering—namely, installing fewer, but more powerful units. We also test the sensitivity of our model under controlled simulation conditions (e.g., fixed tornado path size and the relative position between wind turbines and tornado path). Concluding remarks are provided in Sect. 4.

2 Data and model construction

2.1 Tornado database and climatology

We used a historical database for German tornadoes from 1970 to 2021. This database is available via the European Severe Weather Database (ESWD) (ESWD 2022; Dotzek et al. 2009). For every tornado event, it provides the date, the initial latitude and longitude location, and other fields that are not of interest to this study. It is relevant to note that for 51.5% of the events, the intensity, given in F scale (Fujita 1971), is not provided. In the absence of more information, an intensity F0 is given to the events that lack an intensity rating. Since the F scale is a subjective rating that is based on the quantity, type, and degree of damage caused, it makes sense to assume that an observed tornado with no known casualty would receive the lowest intensity rating. This is also consistent with a policy mentioned by Brooks (2004) that was made in 1982 and meant to assign F0 to all tornadoes that do not have rated damage. However, as discussed by Schaefer et al. (1986), we note that the inconsistencies in the database, combined with the subjective intensity evaluation, introduce a possibility of bias. However, this is a common issue in many studies that rely upon an official severe weather database (ESWD 2022; Dotzek et al. 2009; Romanic et al. 2022). The only reliable way to remove this bias would be to improve the quality of the database. Note that from now on, tornado intensities mentioned as F0 are either categorized as per the database or assumed as per the explanation above and will not be distinguished.

Because of the changes in reported tornadoes over the years, a change-point detection method (Romanic et al. 2020) is used to identify abrupt changes in the annual number of tornadoes (Fig. 1). We observe an abrupt change in the mean annual number of tornadoes between 1970 and 1998, and between 1998 and 2021. Given that these types of abrupt discontinuities are artificially caused, rather than being a result of a natural process (Elsner et al. 2013; Edwards et al. 2013), we only consider the years post-1998 (inclusively). This 24-year-long interval is close to a climatological standard (30 years) and deemed as a sufficiently large sample for Monte Carlo simulations of the annual number of tornadoes.

As demonstrated by Thom (1963), Elsner et al. (2014) and Strader et al. (2017) and also implemented in Romanic et al. (2016) and Refan et al. (2020), the annual frequency of tornadoes is properly represented using a negative binomial distribution (Fig. 1b). The distribution parameters in our model are $r = 8.63$ and $p = 0.15$. From this distribution, the model uses the Monte Carlo method to pseudo-randomly generate an annual number of tornadoes and thus restricts the simulated climatology to that of the database (i.e., observations).

2.2 Spatial distribution and direction of tornado tracks

For each simulated year, the model first generates an annual number of tornadoes (n_y), as described in Sect. 2.1), and then randomly samples n_y reported events from the database. The intensity (F scale) and initial longitude and latitude of the sampled events are further used in the simulations in the following way. We generate a pair of pseudo-random numbers from a normal distribution to randomly nudge the longitude and latitude coordinates of an observed event that was randomly sampled from the database. Using this approach, we preserve the spatial distribution of tornadoes across Germany while simultaneously introducing randomness into their reported positions (Fig. 2). This methodology is an improvement from generating random points uniformly across a geographic region because it aims to follow the observed climatology of tornadoes. Furthermore, this approach also avoids the issue of randomly sampling points on a sphere (i.e., the convergence of longitudes at

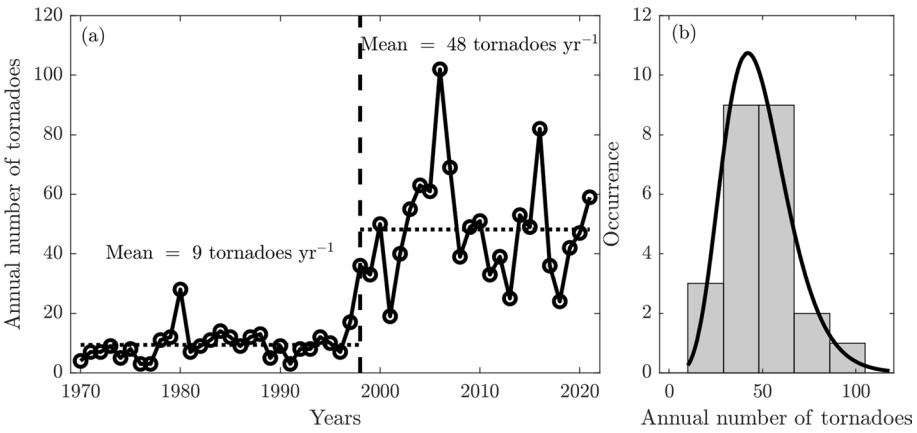

Fig. 1 **a** Annual occurrence of all registered tornadoes over Germany from 1970 to 2021. **b** Histogram of the annual number of tornadoes in the period 1998–2021 fitted with a negative binomial distribution

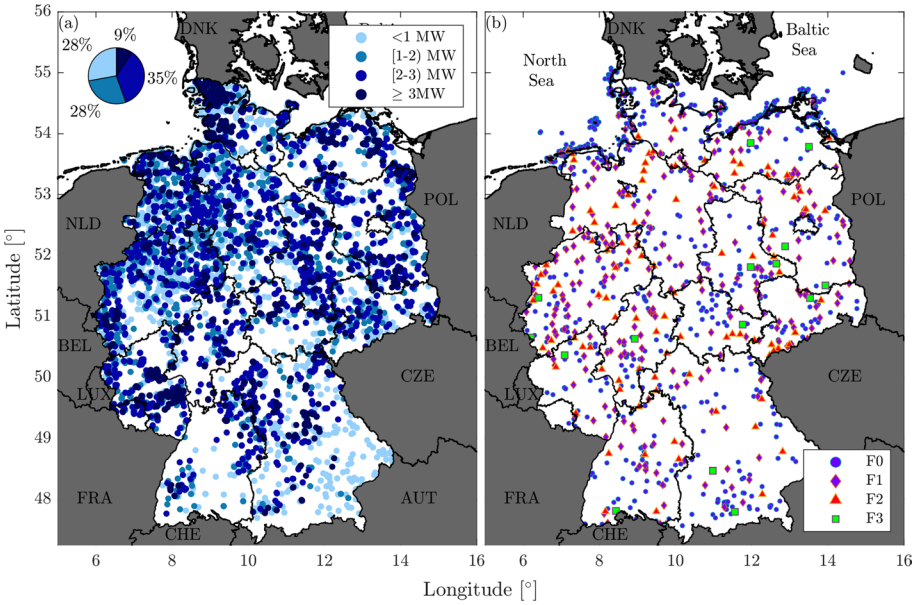

Fig. 2 Map of Germany showing **a** wind turbine locations and their nominal power, including a pie chart of the proportion of different installed capacities in the total number of wind turbines; and **b** tornado locations categorized by their F scale intensities

the poles) versus a flat plane, which is important for large regions that span over several latitudes (Strader et al. 2016).

A kernel density estimator (KDE) is often used to represent the spatial distribution of tornadoes over a region in the absence of a commonly recognized density distribution. Fan and Pang (2019) discussed that the KDE approach is among the most used techniques for spatial analysis of tornado occurrence. They implemented a bi-variate normal distribution as the KDE in their simulation of geographically dependent tornado locations. Similarly, our nudging parameter is based on a normal distribution in both longitudinal and latitudinal directions; hence making the same assumption as Fan et al. that there is no correlation between the two directions. These results will further be discussed in Sect. 3. The present implementation of the KDE in our model does not account for possible spatial correlation between multiple tornadoes such as a tornado outbreak. Tornado outbreaks are challenging to implement into hazard models due to the lack of data associated with the statistical characteristics of tornadoes during an outbreak. More data on the frequency of occurrence of tornado outbreaks, the average number of generated tornadoes and their intensities per outbreak, favorable locations for outbreaks, et cetera, are needed before outbreaks can reliably be implemented into the model. In that case, for example, Ripley's K-function could be used to distinguish between random, clustered, and regular spatial patterns of tornado occurrence.

We also observed that 31% of the tornadoes in the database were located above water (e.g., seas, lakes, or rivers). In all instances, their intensity was F0. Even though we are interested in damage to onshore wind turbines and F0 tornadoes including waterspouts are unlikely to affect the losses calculated by this model, the offshore regions cannot be neglected when the model simulates tornado locations in order to preserve the annual

number and spatial distribution of tornadoes over Germany in accordance with the observations. Thus, to restrict the simulated tornadoes to remain within the lands and territorial waters of Germany after perturbing the observed initial locations of reported tornadoes using the bi-variate KDE method, the model generates tornado events until the longitude and latitude pairs of all n_y events are within Germany's territory.

Hagen and Finke (1999) investigated the prevailing path of thunderstorms using a lightning position system during the summer months of the years 1992–1996 over southern Germany. We used their results to reconstruct tornadoes' bearing angles (i.e., the horizontal angle between the North and the direction of movement, θ) in our study (Fig. 3a). In Fig. 3a, we implement a kernel probability distribution with a normal kernel smoothing function (K) and an optimized bandwidth (h) of 15° to fit their data (of size n).

$$f(\theta) = \frac{1}{nh}\sum_{i=1}^{n} K\left(\frac{\theta - \theta_i}{h}\right) \tag{1}$$

The mean of the fitted distribution is 242° with standard deviation of 58.2°. Hagen and Finke (1999) reported that the most frequent bearing angle of storms is 240°. Figure 3b shows 100 bearing angles generated pseudo-randomly from this kernel distribution. A similarity between the modeled and observed angles is apparent. Moreover, in Fig. 3c, a histogram of the reported bearing angles in the ESWD database since 1998 (corresponding to 27% events of the database) is also shown. While we observe that both sources depict the same prevailing direction of storms toward the northeast ($\theta = 250°$), we used Hagen and Finke (1999) data to construct the pseudo-random number generator of this process due to their larger sample compared to the limited number of ESWD reports.

2.3 Wind speeds and tornado tracks lengths and widths

The distribution of widths and lengths of tornado paths per their intensity is shown in Fig. 4. Here, we further compared the ESWD data for Germany to of tornado's path length and width over the USA from Brooks (2004). In both regions, the length and the width of tornado paths tend to increase with the intensity of tornadoes (Fig. 4). Despite the two

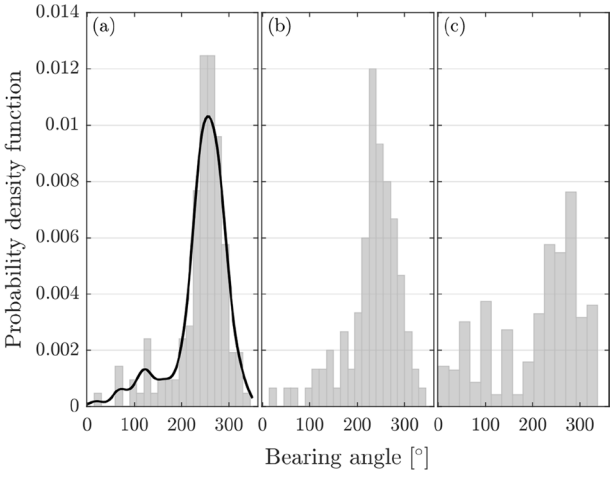

Fig. 3 **a** Empirical histogram and modeled kernel distribution of bearing angles of storm trajectories over Germany (Hagen and Finke 1999). **b** Distribution of the bearing angles from a 100-year simulation run of our model. **c** Distribution of bearing angles of tornado tracks from the ESWD database (ESWD 2022)

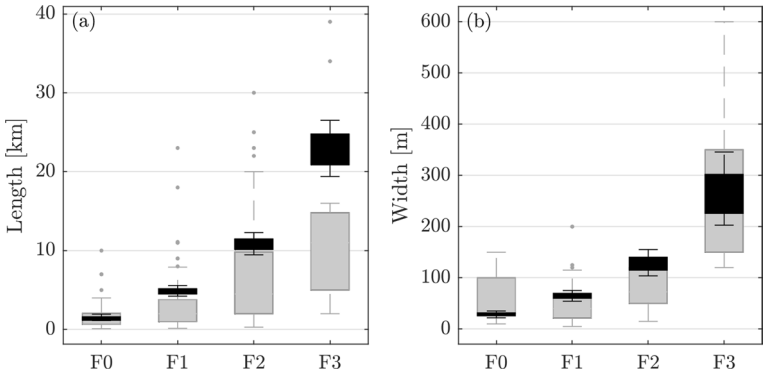

Fig. 4 Box-and-whiskers plot of tornadoes' paths for **a** path lengths, **b** path widths. Gray boxes represent the ESWD database for Germany (GRAY points as outliers) and black are the US data (Brooks 2004)

regions being climatologically different, the geometry of their tornado paths is similar. Dessens and Snow (1993) showed that tornadoes in France have mean path sizes similar to tornadoes in the USA. They further suggested that if path data of all tornadoes that occurred in France were available, the statistical trends of tornadoes in the USA and in France would likely be even more similar. We argue that similar conclusions should hold for Germany too. Therefore, our model makes use of Brooks' results to simulate tornadoes' path lengths and widths using a Weibull distribution:

$$f(p_{w,l}) = \left(\frac{\alpha}{\beta}\right)\left(\frac{p_{w,l}}{\beta}\right)^{\alpha-1} \exp\left[-\left(\frac{p_{w,l}}{\beta}\right)^{\alpha}\right], \tag{2}$$

where $f(p_{w,l})$ is the probability density function of tornado path width or length $p_{w,l}$ (here, $p_{w,l}$ can be either the path length or the width for a given F scale), $\alpha > 0$ is the shape parameter and $\beta > 0$ is the scale parameter (Table 1).

Weibull distributions have been used repeatedly in literature to represent wind speeds in different regions around the globe as well as wind speeds associated with different types of wind events (Justus et al. 1976; Seguro and Lambert 2000; Brooks 2004; Ghosh and Rafkin 2012; Standohar-Alfano and Lindt 2015; Romanic et al. 2018, 2020). Similarly, Weibull distributions have been found to properly model tornado's path length and width (Brooks 2004; Dotzek et al. 2003; Meyer et al. 2002).

Given that there has not been a tornado with a rated intensity stronger than F3 in the ESWD database in the period 1998–2021 over Germany, the presented model will therefore never simulate an F4 or F5 tornado. That is, the simulated tornadoes are sampled from the database.

Table 1 Weibull distribution parameters of the length and width of tornado paths (Brooks 2004): α is the shape parameter, β is the scale parameter and μ is the mean of the distribution. β and μ are given in meters for width and kilometers for length

F scale	Width			Length		
	α	β	μ	α	β	μ
0	0.94	27.2	28.4	0.65	0.9	1.4
1	0.85	57.7	64.0	0.62	3.1	4.7
2	0.79	107.4	125.9	0.64	7.5	10.7
3	0.84	240.2	263.6	0.83	20.4	22.5

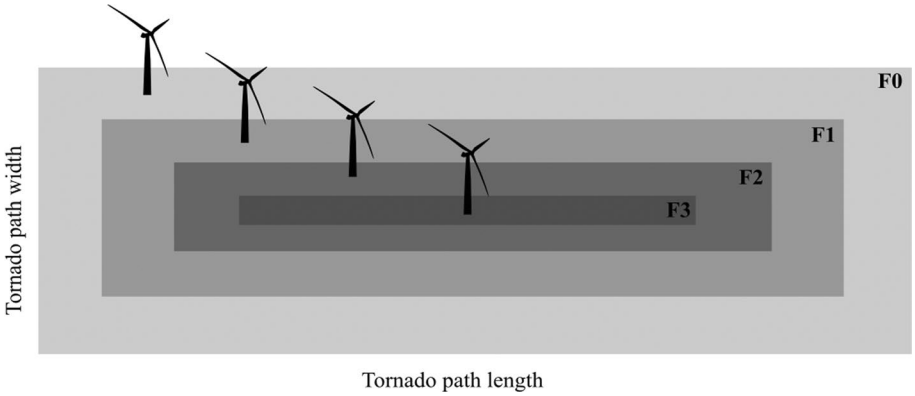

Fig. 5 Blueprint of a segmented F3 tornado (not to scale) (Standohar-Alfano and Lindt 2015). The illustrated wind turbines are subjected to four different wind speeds, each wind speed corresponding to different F zones

Though the possibility that such a tornado could occur over a sufficiently long time period is, of course, not excluded given that F4 tornadoes did happen before 1998 (Dotzek 2001), this scenario does not affect the outcome of our model because F3 tornadoes already cause the maximum damage to wind turbines (Marshall et al. 2022). This topic is further discussed in Sect. 2.5.

A proper representation of the variability of tornado intensity during their lifetime is important to adequately model the monetary losses caused by this type of non-stationary wind hazard. Schaefer et al. (1986) analyzed the tornado variation in intensity (F scale) versus length for 5 surveyed tornado outbreaks in the USA (cf. Table 2 in Schaefer et al. (1986)). Standohar-Alfano and Lindt (2015) combined the work of Schaefer et al. (1986) with additional tornado damage surveys and proposed a method to account for a tornado variability in intensity along the length and the width of the tornado path. They summarized the variability by segmenting the footprint into zones of different intensity magnitudes. Each segment is rectangular in shape and defined as a percentage of the total length and width of the tornado path (Fig. 5). Because their model was constructed using mixed data that did not distinguish between F and Enhanced F (EF) (McDonald et al. 2006) tornado intensity ratings, they considered both classifications to be equivalent in terms of the variation of tornado intensity along the path. Similar to Romanic et al. (2016), we adopted the method of Standohar-Alfano and Lindt (2015) herein.

It is arduous to analyze tornado wind speeds because they cannot be routinely measured. Instead, wind speeds are inferred from the damage caused by tornadoes. This method is also often uncertain due to structural and construction differences of the "standard" structures from which damage can be assessed (McDonald et al. 2006). Moreover, wind speeds vary along the track of a tornado, as discussed above, and these wind gradients are even harder to estimate. Because no wind speed data was available in the ESWD database, we assumed similar wind speed distributions for tornadoes in the USA and Germany, and, therefore, used Elsner et al. (2014) wind speed simulations to estimate a distribution of wind speeds across tornado F segments. Elsner et al. (2014) investigated tornado intensities on a continuum by estimating wind speed based on damage, path dimensions, and EF ratings. We use their model diagnostic plot (cf. Fig. 3a in Elsner et al. (2014)) to obtain a distribution of tornado wind speeds in our model. Weibull, log-normal, and gamma distributions were applied to Elsner et al.'s data

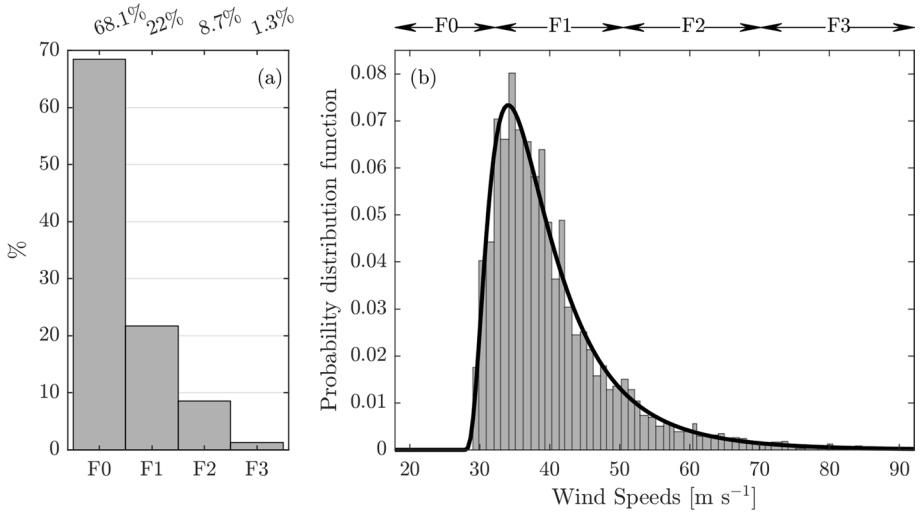

Fig. 6 **a** Percentage occurrence of tornadoes per their F scale over Germany. The values at the top of the plot represent the observed percentages in the ESWD database. **b** Distribution of wind speeds as a function of tornado intensity based on the model by Elsner et al. (2014) with the log-normal fit added (black line)

using the maximum likelihood method and the log-normal distribution provided the best fit of data with a Chi-square (χ^2) of 0.022 (Fig. 6b). Log-normal distributions are appropriate to model tornado wind speeds since they are non-negative and positively skewed (Fig. 6). The probability density function of a log-normal distribution that models wind speeds (v) as a random variable is:

$$f(v) = \frac{1}{\sqrt{2\pi}\sigma v}\exp\left[-\frac{1}{2}\left(\frac{\ln(v)-\mu}{\sigma}\right)^2\right], \tag{3}$$

where μ is the scale parameter (i.e., the median of the distribution) and σ is the shape parameter. Because the lowest wind speed in an F0 tornado is 18 m s^{-1} by definition, a location parameter (θ) is added to the log-normal distribution to account for the cut-in wind speed, as:

$$f(v) = \frac{1}{\sqrt{2\pi}\sigma(v-\theta)}\exp\left[-\frac{1}{2}\left(\frac{\ln(v-\theta)-\mu}{\sigma}\right)^2\right]. \tag{4}$$

In our model, σ, μ and θ parameters are 2.32, 0.66 and 27.52, respectively. Within each F zone (e.g., Fig. 5), wind speeds at locations of the affected wind turbines are pseudo-randomly generated from log-normal distribution within the bounds of wind speeds associated with a given F scale.

2.4 Exposure map

Exposure map of onshore wind turbines over Germany (Fig. 2a) is obtained from the Helmholtz Centre for Environmental Research (UFZ) data research portal (UFZ 2019;

Eichhorn et al. 2019). Their data from 2015 provide wind turbines (24,475 units in total) Northing and Easting coordinates (ETRS 1989 geodetic Cartesian reference frame), the nominal wind turbine capacity in kilowatts (kW), and other attributes of installed wind turbines that are not relevant to this study. 18 wind turbines were associated with a 0 kW capacity and were removed from the analysis to avoid unnecessary speculation. The only instance of an offshore wind turbine was also eliminated such that the final exposure map consists of 24,456 wind turbines. The highest concentration of wind turbines is found in the north and northwest parts of Germany.

2.5 Vulnerability and loss assessments

Vulnerability functions are a quintessential part of risk assessment models. In our model, the vulnerability function describes the relationship between a tornado's wind speed and expected damage to a wind turbine. The damage is quantified through a damage index (D) which is a percentage of the replacement or full reparation of a wind turbine. The maximum damage ($D = 1$) is associated with a collapse of the wind turbine or damage so severe that the full replacement of the unit is necessary even if some components of the wind turbine are in place. A damage index of $D = 0$ represents no damage inflicted to a wind turbine (Fig. 7).

Vulnerability functions are not expected to be accurate for a single incident, but rather to overlay the global pattern of events for a particular type of phenomenon and structure (Walker 2011). Therefore, vulnerability curves are often the main source of uncertainty in a hazard model. In fact, a significant amount of data is required to empirically develop a reliable vulnerability curve, but due to high variability in the events (e.g., different spatiotemporal characteristics of tornadoes, the orientation of their trajectories relative to a wind turbine, orographic influences, flying debris, pressure deficits in the tornado core, etc.), different wind turbine characteristics (e.g., size and hub height, rotor diameter, soil properties and type of foundation, material, building standards, etc.) and limited pool of damage surveys, composing a highly reliable vulnerability model is

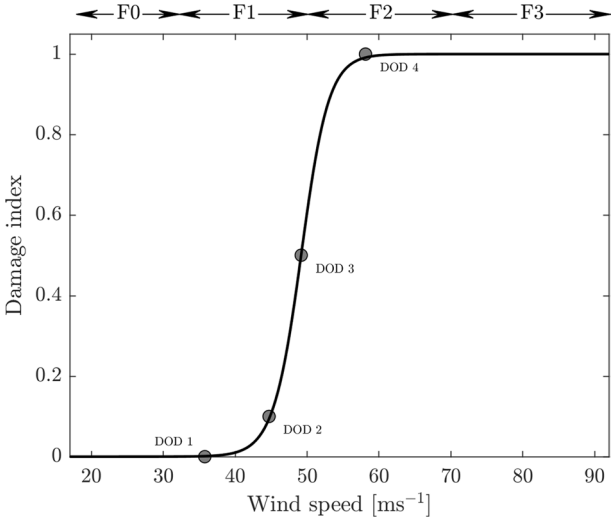

Fig. 7 Vulnerability curve. Degrees of Damage (DOD) Marshall et al. (2022) is associated with the expected lower bounds of damage index and resistance wind speeds

always challenging. Some of these issues are further discussed in Romanic et al. (2016), Walker (2011) and Papathoma-Köhle et al. (2012).

Surveys of wind turbine damage caused by tornadoes that will be included in the updated EF scale recommendation report (Marshall et al. 2022) provide a quantitative relationship between typical resistance wind speed and a given degree of damage (DOD) inflicted to a wind turbine (Table 3). DODs are categorical measures (0–no damage to 4–highest damage) of the severity of the damage that a wind turbine sustained in a tornado. Here, we propose a generalized logistic function—the so-called Richard's curve—to develop a continuous vulnerability function from discrete DOD points (Fig. 7):

$$D(v) = \beta + L\left(1 + Ie^{-k(v-v_m)}\right)^{-1/I}, \tag{5}$$

where β is the lower asymptote ($D = 0$), L is the upper asymptote ($D = 1$), v_m is the point of maximum growth (49.1 m s^{-1}), k is the growth rate (0.504) and I is a variable associated with the point of inflection (0.970). Cumulative distribution functions in the form of Eq. (5) are appropriate choices of models to construct vulnerability curves as they define DOD in a both-sided defined interval and are steady monotonic increasing functions (Papathoma-Köhle et al. 2012). Other types of cumulative distribution functions (e.g., Weibull, log-logistic, Frechet, and logistic) have also been used in literature to develop vulnerability curves for other hazards (Papathoma-Köhle et al. 2012; Totschnig and Fuchs 2013; Totschnig et al. 2011). In our case, five parameters of the generalized logistic function facilitate the curve fitting of limited DOD data more easily than employing other cumulative distribution functions with fewer degrees of freedom.

Figure 7 implies that no damage is caused by F0 tornadoes and that total destruction is expected for F3 tornadoes. As previously mentioned, this implies that F3 and higher tornadoes equally affect wind turbines in terms of losses as the damage cannot exceed $D = 1$. Figure 7 also depicts the largest variability in the damage caused by F1 ($0 \leq D < 0.6$) and F2 ($0.6 \leq D \leq 1$) tornadoes.

The final module of our model is the loss calculations by which the physical damage described by the vulnerability curve (Fig. 7) is linked to financial losses (€). Each DOD state that was used to develop our vulnerability curve provides a qualitative description of the damage that a wind turbine is expected to sustain in tornadoes (Table 2). These estimates are based on surveyed wind turbines affected by tornadoes. We combined this information with the estimates of the typical cost of replacement of different wind turbine components as a function of the total cost of a wind turbine (P) of a nominal capacity C (Blanco 2009; Martin-Tretton et al. 2022; WISDEM 2019) (Table 3). While Blanco (2009), Martin-Tretton et al. (2022) and WISDEM (2019) provide similar estimates of the cost of different wind turbine components, there are also some differences in their assessments due to a variety of wind turbine types and manufacturers on the market (Blanco 2009).

In our model, the total cost value of a wind turbine (V) that includes all components, grid connection, engineering work, licensing, and other costs is calculated as:

$$V = C \cdot R, \tag{6}$$

where R is a typical price of a wind turbine per kW of nominal power. Here, R is generated pseudo-randomly from a normal distribution with the mean of 1,250 € kW^{-1}, standard deviation of 15% and, following the work of Blanco (2009), the values are bounded

Table 2 Main components of a typical horizontal axis onshore wind turbine and their percentage contributions to the total capital cost (Blanco 2009)

Component	%	Description
Tower	26.3	Structure supporting the wind turbine
Rotor blades	22.2	Airfoil shaped blades that "capture" wind energy and drive the rotor
Rotor hub	1.37	Holds the blades in position as they turn
Rotor bearings	1.22	Balance the various forces imposed by the wind
Main shaft	1.91	Transfers the rotor torque to the gearbox
Main frame	2.80	Supports the turbine drive train
Gearbox	12.9	Boosts the low rotational speed of the shaft for the generator
Generator	3.44	Converts mechanical energy to electrical energy
Yaw system	1.25	Rotates the nacelle in an optimal way
Pitch system	2.66	Adjusts the angle of the blades in an optimal way
Power converter	5.01	Converts the direct current to alternating current for the grid network
Transformer	3.59	Converts the electricity to a higher voltage for the grid network
Brake system	1.32	Pauses the functioning wind turbine when needed.
Nacelle housing	1.35	Covers the turbine drive train
Cables	0.96	Links the wind turbine to an electrical station
Screws	1.04	Maintain the components in place

Table 3 DODs for wind turbines in tornadoes (Marshall et al. 2022). The wind speeds represent the typical resistance wind speed (3-second gusts) for a given DOD. A higher DOD incorporates the damage of lower DODs

DOD	Affected components	v [m s^{-1}]
0	No damage	<36
1	Brake system including cables and screws	36
2	Blade(s), rotor hub, rotor bearings, gearbox, pitch system	45
3	Generator, nacelle, main shaft, yaw system, main frame, small damage to tower	49
4	Entire wind turbine collapses	58

between 1,100 and 1,400 € kW^{-1}. The nominal capacity, C, of each wind turbine within the exposure map is provided in the UFZ database (UFZ 2019; Eichhorn et al. 2019) (Fig. 2a).

The monetary loss associated with a damaged wind turbine (L_{wt}) is:

$$L_{wt} = \begin{cases} D(v) \cdot V, & \text{if} \quad D < 0.7; \\ V, & \text{if} \quad D \geq 0.7. \end{cases} \tag{7}$$

Naturally, L_{wt} is zero for F0 tornadoes as well as F0 tornado zones in the peripheral regions of stronger tornadoes (Fig. 5), which also includes any tornadic wind speeds $v < 36$ m s^{-1} (Fig. 7). On the other hand, $L_{wt} = V$ for $v \geq 58$ m s^{-1}. Moreover, if $D \geq 0.7$, the loss is still deemed to be V because such a high level of sustained damage to a wind turbine requires the entire unit to be replaced. Indeed, considering that the tower contributes to

approximately 30% of the value of V (Blanco 2009), the total replacement of the unit for $D \geq 0.7$ is regarded as a reasonable estimate of the loss for the most severe levels of damage.

While a deterministic relationship between wind speed, damage, and loss is the simplest way to link these parameters, we also propose and test an alternative approach to model D and therefore L_{wt} too. To account—at least partially—for various uncertainties associated with vulnerability and damage estimates as a function of tornadic wind speeds, we also allow for damage to be normally distributed around the mean values calculated by the deterministic Eq. (5). Then, we used a standard deviation of 15% (Romanic et al. 2016) to pseudo-randomly sample the final value of D that was used to calculate losses in Eq. 7. The upper and lower limits of a random sampling of D are set to be 1 and 0, respectively, in order to suppress non-physical results. This approach attempts to further generalize the derived vulnerability function to a large number of possible wind turbine-tornado interaction scenarios.

The total loss caused by a tornado event (L_{event}) is the sum of L_{wt} losses of all wind turbines affected by the tornado. Finally, the aggregated loss (AGG) is the sum of all L_{event} losses in the year, and the largest L_{event} loss in the year is the so-called occurrence loss (OCC). These definitions are borrowed from the insurance sector (Romanic et al. 2016). AGG and OCC are used to derive tail risk values for risk management of expected losses, which are further linked to different return periods (RPs). RP is defined as the one over the cumulative likelihood such that a 1% likelihood of exceedance of a loss is given an RP of 100 years (Romanic et al. 2016).

3 Results and discussion

3.1 Tornado spatiotemporal occurrence

The negative binomial distribution of the annual occurrence of observed tornadoes yields a mean of 48 events per year (Fig. 1b). A kernel smoothing function estimation was performed on 5 runs of 100-year simulations to compare the simulated spatial occurrence of annual occurrence of tornadoes with observations (Fig. 8). The estimate is based on a bivariate normal kernel function to remain consistent with the methods. It seems that the spatial density of the simulated tornadoes is coherent with the database for F0 and F1 tornadoes. Figure 8 also projects noticeable variability for the F2 category and even more pronounced irregularities for F3 tornado locations, suggesting a poorer ability of the model to reproduce F2 and particularly F3 tornado climatology. These observations suggest that, while reproducing the spatial distribution of tornado occurrence can improve the adequacy of a model when a sufficient amount of data is available, this method might also be a drawback when only a few records exist (in this case 100 F2 and 15 F3 tornado records). Nevertheless, relative frequencies of tornado intensity are similar to observations as shown in Fig. 6a.

More than two-thirds of the total number of observed tornadoes over Germany in the period 1998–2021 belong to the weakest twisters; a similar ratio is obtained for 30 runs of 1000-year simulations (68.4%). This finding suggests that only about a third of the annual tornadoes have the potential to be damaging to wind turbines. Nearly 10% of the events are severe (F2 and stronger tornadoes) and can result in drastic damage or the complete collapse of wind turbines (Fig. 7).

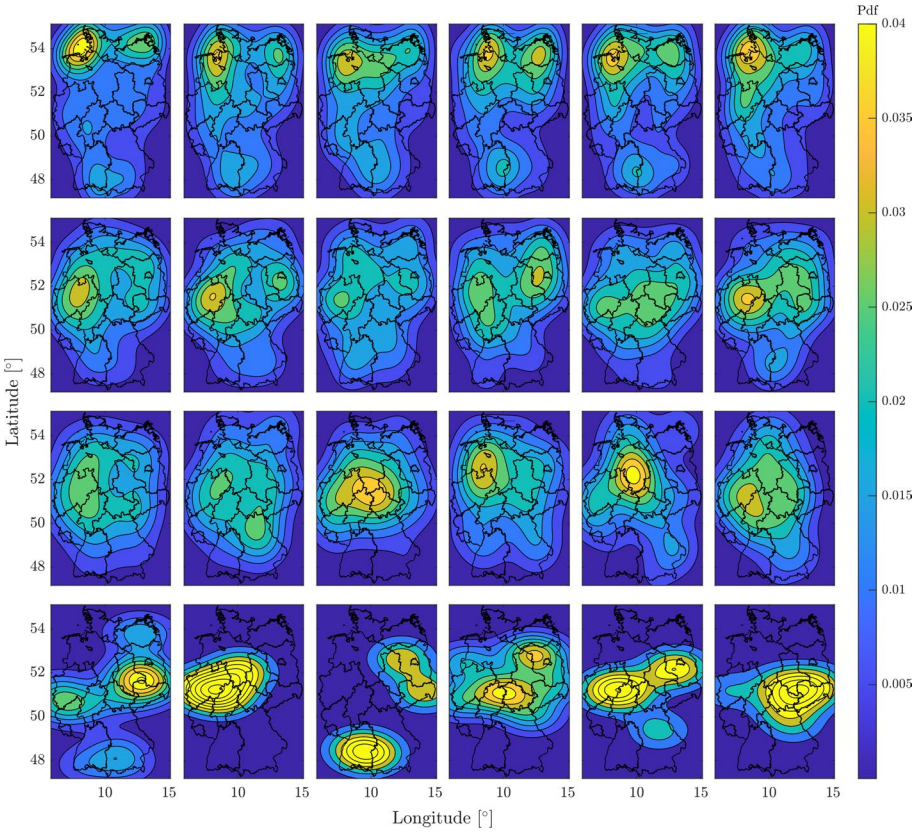

Fig. 8 Normal bi-variate kernel density estimators of the spatial occurrence of tornadoes across Germany. Each row represents a different F scale (F0 to F3 starting from the top). The left column is tornado climatology from the ESWD database, and the subsequent columns are based on model runs

Tornado tracks over Germany are shown in Fig. 9 for a different number of simulated years. The total number of tornadoes is coherent with the annual mean. In the six presented cases, the annual number of tornadoes ranges between 43 and 51. The 500- and 1000-year simulations show that the pseudo-random selection of tornado initial locations, based on a KDE of the observed tornado spatial occurrence, results in a tendency to favor certain regions based on the observed climatology. Namely, weak tornadoes (F0–F1) are predominant in northwestern Germany, whereas stronger tornadoes (F2–F3) seem to appear mostly in the mid-west and east sectors. The south seems to be the least favored region for tornadoes (Fig. 8).

In terms of the prevailing bearing angle of tornado tracks, the mean direction of the simulated tornadoes ($\theta = 242°$, which also corresponds to the mean of our fitted kernel distribution), our simulations agree well with the most frequent bearing angle of storms observed by Hagen and Finke (1999), $\theta = 240°$. While the modeled angles are independent of the tornado intensity in this work, we acknowledge that the intensity and the orientation of tornado tracks might be dependent parameters. Having more data on tornado paths would improve the accuracy of the model to depict the orientation patterns of tornadoes, rather than relying on thunderstorm trajectories.

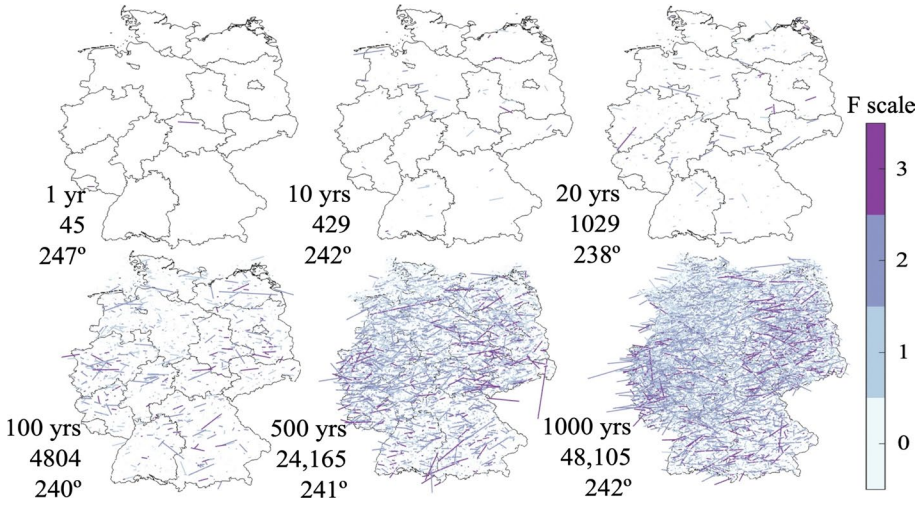

Fig. 9 Modeled tornado tracks over Germany for return periods of 1, 10, 20, 100, 500, and 1000 years. The total number of modeled tornadoes and mean bearing angles of tornado tracks are indicated in the bottom-left of each figure

Tornadoes are the most active through the summer months when the electricity production by wind turbines is the smallest (Fig. 10). Between 2000 and 2014, the mean capacity factor of wind farms in Germany was around $18.3 \pm 7.5\%$ (Germer and Kleidon 2019) with values over 40% occurring only occasionally in the winter months. Seasonal decoupling between tornado occurrence and mean capacity factors, which are slightly above 10% during the summer (Fig. 10), is beneficial in terms of potential disruption of a wind farm operation and associated financial burden that wind farm owners might sustain if we equate

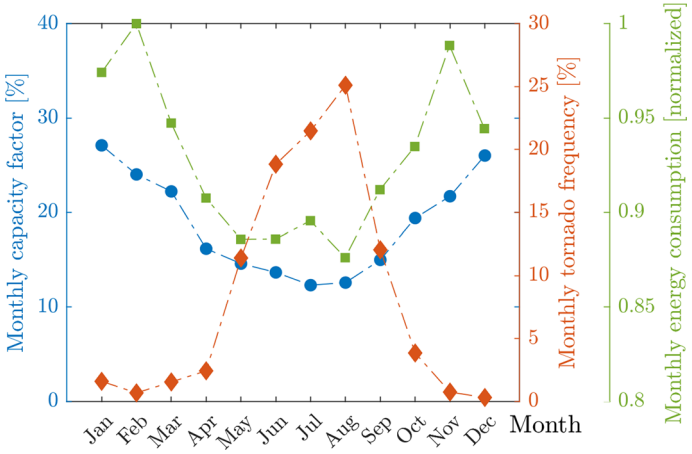

Fig. 10 Monthly capacity factors of wind farms in Germany (left *y*-axis, blue) Germer and Kleidon (2019), normalized energy consumption in Germany (second right *y*-axis, green—normalized to the peak value of 58,993 MWh in February) Bach (2022) and relative frequencies of the monthly number of tornadoes over Germany (first right *y*-axis, red)

the smaller capacity factors with reduced revenues from the exported electricity to the grid. However, from the energy consumption point of view, the high frequency of occurrence of tornadoes in summer months might be problematic given that the minimal consumption in August is only 12% smaller than in the peak month of February (Fig. 10). That is, the high demand for electricity is maintained throughout the year. Germany is rather specific in this regard because, for example, the load in summer months in France is ~35–40% lower than in the winter months (not shown) (Bach 2022).

3.2 AGG and OCC losses

The model uses two methods to simulate losses (Sect. 2.5): (1) a deterministic relationship (DR) between D, wind speed, and loss; and (2) added randomness in the deterministic relationship (RDR). The AGGs and OCCs are computed for both methods and illustrated in Fig. 11 as a function of the RP.

Both curves are steep for the RPs below 200 years and approach the highest expected losses for larger RPs. Nevertheless, positive gradients are still observed on the curves for RP = 1000 years, suggesting AGGs and OCCs should flatten at values larger than 25 M€. In other words, losses with higher RPs can be expected. The results seem to diverge in the tail region of the curves. Also, the AGG losses calculated using the DR method show more spread around the mean. This suggests that the choice between using the deterministic (DR) or random-deterministic (RDR) approach to estimate the relationship between wind turbine damage and wind speed is less significant for high-frequency events (i.e., small RPs), but becomes more relevant for lower frequency losses (i.e., large RPs). The low-frequency events, however, are particularly important considerations for insurance and reinsurance underwriters in the wind energy sector. We also notice that the lower-bound losses in the DR approach already cap at the RP of approximately 500 years. Larger uncertainty of the tail losses is associated with the DR approach and, also, the tail OCC losses of the DR method are larger than for the RDR method in the tail region (Fig. 11).

Given the S-like shape of the vulnerability function (Fig. 7), the RDR method tends to augment the losses for weaker tornadoes (low-end F1) and reduce them for strong tornadoes (upper-end F1 and lower-end F2). For example, consider a wind speed of 40 m s^{-1} and the associated damage index of $D_{DR} \approx 8.5 \times 10^{-3}$ (i.e., negligible in the DR approach).

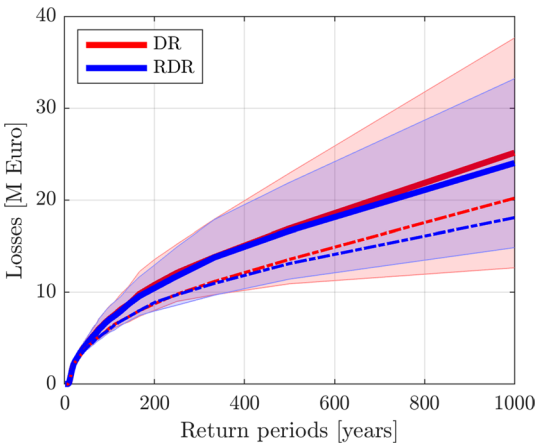

Fig. 11 Probability exceedance curves showing AGG (full lines) and OCC (dot-dashed lines) losses associated with the DR (red) and RDR (blue) vulnerability modeling methods. The profiles are based on an average of 60 1000-year RP model runs. The shaded regions represent one standard deviation around the mean AGG losses

In the RDR model, however, a new value of D_{RDR} will be re-sampled from a normal distribution with the mean of D_{DR} and a 15% standard deviation. Given that D_{DR} is already small, a potential re-sampling toward even lower values does not affect the loss significantly because of the small slope of the vulnerability function in that region and, moreover, the damage is capped at 0. However, the steep slope of the vulnerability curve toward higher damage than D_{DR} can significantly increase the damage and consequently the loss. The reader can convince themselves that the opposite argument holds at the high end of the vulnerability curve (Fig. 7).

This trend is particularly observed in the mean OCC losses (Fig. 11) that are higher in the DR approach over the tail region of the probability exceedance curves. The variability of RDR model is smaller in the low-frequency range. For both methods, the losses are bounded by V if $D > 0.7$. Since RDR re-samples D normally, but caps the losses equivalently to DR, we expect the extreme cases of RDR to be slightly smaller than DR on average as the method often re-samples smaller values and both methods are equally bounded at the high end. Similarly, as D is bounded below by 0 in both DR and RDR models, we expect RDR to re-sample D slightly positively for the small loss events (i.e., small D) on average. While this property of the vulnerability models affects the calculated losses across the probability exceedance curves, the influence is more noticeable in the high-frequency range due to a large number of high D_{DR} damage states of affected wind turbines in these extreme years and prior to their D_{RDR} re-sampling.

3.3 Modified exposure map: increased number of units and repowering

Considering Germany's goal to double the onshore wind turbine energy production by 2030 (GTAI 2022), we analyzed two different scenarios of the modified exposure map: (1) doubling the number of units while following a similar capacity distribution as the presently installed wind turbines (2NUM); and (2) installing fewer but more powerful units, which also addresses the inclination toward the so-called repowering (2CAP). The added wind turbines in the 2NUM case are uniformly distributed following random sampling on a sphere across the exposure map. Capacities of new wind turbines are randomly sampled with replacement from the existing database (see Fig. 2). A somewhat simplified portrayal of Germany's future wind turbine exposure map is implemented for 2CAP. We use the 100 GW goal (GTAI 2022) as the total onshore wind energy capacity of Germany and normally randomize individual wind turbine capacities. According to the International Renewable Energy Agency (IRENA 2019), ongoing innovations and enhancement for the wind energy sector is expected to shift the international average of capacities for individual units from 2.6 MW to 4–5 MW for turbines commissioned by 2025. Because this report dates from 2019 and technologies have improved since then, and also given that 7.5 MW onshore wind turbines are now operational on Magdeburg-Rothensee and Ellern onshore wind farms in Germany, we use a mean nominal power of 5.2 MW and restrict capacities to be within 4 and 8 MW. Thereby, the mean of 5.2 MW with a 15% standard deviation are used to normally randomize the 2CAP wind turbine capacities. This way, the initial number of wind turbines (24,456) is reduced by about 27%, which is an appropriate figure for doubling wind farm capacities with the repowering method. The locations of the repowered turbines are randomly sampled without replacement from the existing wind turbine exposure map.

Figure 12 shows the AGG and OCC losses associated with 2NUM and 2CAP using the DR method. The significant gradient in the tail losses of both curves suggests higher than

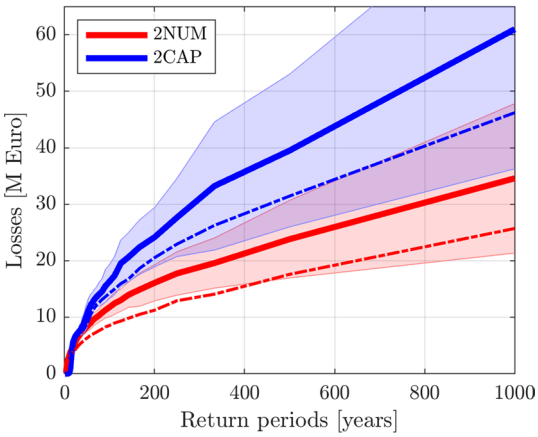

Fig. 12 AGG (full lines) and OCC (dot-dashed lines) loss profiles for modified exposure map: doubling the number of wind turbines with capacities similar to the currently installed units (red) and new repowered wind turbines adding to a total capacity of 100 GW (blue). The results are based on 30 model runs. Similar to Fig. 11, the shaded regions represent one standard deviation around the mean AGG losses

1/1000 AGG and OCC losses. The losses for 2CAP are more significant than the losses for 2NUM across the exceedance curves and nearly double the 2NUM values in the tail region.

This simplified comparison model suggests two outlooks. First, the repowering of onshore wind turbines is expected to yield more significant losses due to tornado damage than increasing the number of existing units. Thus, increasing the capacity (2CAP)—i.e., increasing the monetary value of the units associated with the increased capacity through Eq. 6—contributes more to the losses than increasing the number of intersections between wind turbines and tornadoes caused by the increased number of existing wind turbines (2NUM).

Second, this result shows that our model is particularly sensitive to the installation costs of wind turbines. Therefore, we highlight the importance of more available and standardized data from the wind energy sector in order to accurately depict wind turbines' monetary values and related damage costs. Particularly, there is a lack of data on which wind turbine components are most susceptible to tornadic wind loads and what are the expected modes of failure. One could hypothesize that doubling the number of units does not directly double the potential losses, as the probability of tornadoes hitting wind turbines remains low. However, doubling the capacity would significantly amplify the potential losses because they are intrinsically linked with damage cost in our model. Thus, the 2CAP losses are greater than the 2NUM losses.

Wind turbines are expected to last around $N_y = 20$ years (Salameh et al. 2018; Blanco 2009) and their economic payback period is about $N_y = 10$ years (Blanco 2009). Here, we shall calculate the probability (P) of a tornado hitting a wind turbine in Germany over a period of N_y years. For a wind turbine with a nacelle length s and a rotor diameter d, the horizontal area that the wind turbine sweeps under a 360° yaw rotation is $A_{wt} = \pi R_e^2$, where the effective radius is $R_e = \sqrt{(D/2)^2 + (s/2)^2}$, assuming that the tower and nacelle are connected at approximately the middle of the nacelle length. Furthermore, the area of a rectangular tornado track (Fig. 5) is $A_t = lw$, where l and w are the total length and width of the track, respectively. Under these assumptions, the probability of one tornado hitting a wind turbine (p) is found in two steps: (1) Determining a region, A_{twt}, such that A_{wt} intersects A_t in one and only one point within A_{twt}, and (2) Dividing the area A_{twt} by the total area of Germany ($A_G = 357,588$ km^2). It can be demonstrated that the area A_{twt} is a rounded rectangle with the sides l and w and a corner radius R_e:

$$A_{twt} = lw + 2R_e(l + w) + \pi R_e^2. \tag{8}$$

Therefore, $p = A_{twt}/A_G$ for one tornado. However, given that the average number of tornadoes in a year is N_t, the probability that none of them intersects A_{wt} is $(1 - p)^{N_t}$; hence, the probability at least one of them intersects A_{wt} is $1 - (1 - p)^{N_t}$. For small p, this expression can be approximated as pN_t. The derivation also assumed that $A_G >> A_{twt}$ in order to neglect the effect of irregular border shape. Finally, the probability P of at least one tornado hitting a wind turbine over N_y years is:

$$P = \frac{A_{twt}}{A_G} \cdot N_t \cdot N_y. \tag{9}$$

Under the reasonable assumption that $s = 10$ m, $D = 150$ m, the probabilities for tornadoes of different intensities hitting a wind turbine in Germany are provided in Table 4. The results of Brooks (2004) (see Table 1) on tornado path lengths and widths and a mean of 48 tornadoes year^{-1} (Fig. 1) are used to approximate l, w and N_t, respectively. Interestingly, the probability of a hit by an F0 tornado is lower than the probability of a hit by either F2 or F3 tornadoes. Despite being the most numerous, F0 tornadoes are also the smallest in size, which results in a low probability of the hit. It is also important to note that F0 tornadoes are not causing damage to wind turbines in our model (Fig. 7). The probability of a hit by F1 and F2 tornadoes is similar and approximately two times larger than that of an F3 tornado. Since the calculated probabilities assume a uniform distribution of tornadoes across the exposure map, which is not fully supported by the observed tornado climatology (Fig. 8), the provided figures should be taken as an "average" probability of the hit.

Further research concerning the optimization of the two scenarios (e.g., combining 2CAP and 2NUM) in order to determine the dependency of results on varying different parameters (e.g., mean repowering capacity or the number and locations of added wind turbines) would be particularly interesting to pursue in a future study. The results of that research will also alter the calculated probabilities in Table 4.

3.4 A fixed tornado path

Multiple model runs of a tornado with a fixed length, width, and orientation of the track (Fig. 13) were conducted to investigate the sensitivity of our model to unchanged initial conditions. This fixed path is positioned to traverse an existing wind farm at Schleswig-Holstein, Germany, that has 17 wind turbines—16 of 2 MW capacity and one of 1.8 MW capacity. The location of the wind turbines within the track and the dimension of the tornado track are portrayed in Fig. 13 (not to scale). A total of 18 scenarios, consisting of 30 runs of 1000-year simulations, were executed. These scenarios include varying the tornado intensities (F1–F3), three different capacities of the wind turbines (halved, unchanged, and doubled), and the two vulnerability modeling approaches (DR and RDR).

Table 4 Probabilities in percentages for tornadoes of different intensities (F scale) to hit an average-sized wind turbine in Germany over the period of 10 and 20 years

N_y	P (%)			
	F0	F1	F2	F3
10 years	0.0249	0.0306	0.0349	0.0164
20 years	0.0498	0.0611	0.0699	0.0327

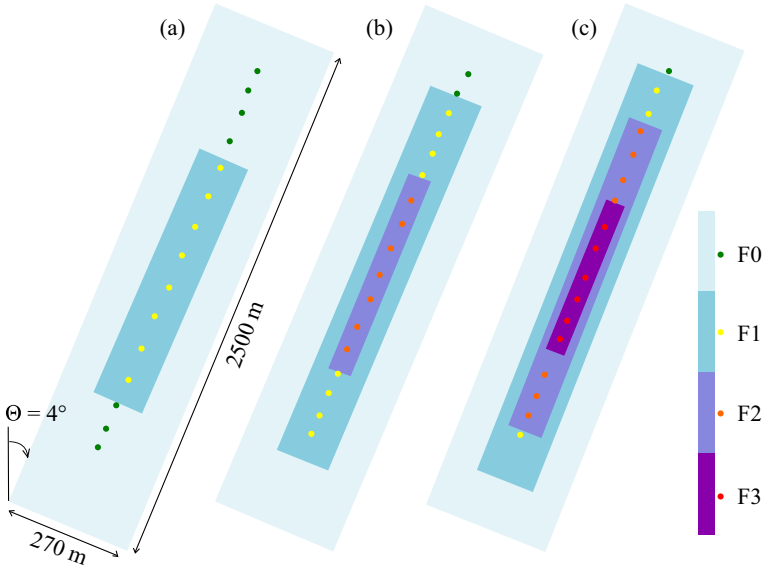

Fig. 13 A tornado track of the fixed size and bearing angle is placed over 17 wind turbines (dots). The bearing angle value of 4° is exaggerated for the sake of better visualization. The tornado F-scale rated intensity is varied from F1 to F3 (**a**–**c**)

The histograms associated with the F1 tornado (the first column in Fig. 14) show no pronounced distinction between the DR and RDR methods. The mean losses scale linearly among the 3 wind farm capacity cases (halved, unchanged, and doubled capacities). This result suggests that a lower range of damage and fewer occurrence of intersections result in similar loss distributions with both approaches. Since the lower bound of F1 wind speeds results in no damage (Fig. 7), the F1 histograms exhibit a Poisson-like shape with the left tail being cut off at a zero loss. On the other hand, the F2 and F3 histograms (the second and third columns in Fig. 14) show a systematic shift from RDR to the DR distributions. The RDR losses are more spread around the mean and lower than the DR losses. This trend can be explained by further examining the vulnerability function (Fig. 7) in terms of the RDR sampling. In the RDR approach, the deterministic damage (DR) is randomly re-sampled from a normal distribution with the mean equal to the DR damage and a 15% standard deviation. For large DR damage states, the losses are already close to the replacement cost, and the RDR re-sampling toward higher losses is capped at the replacement cost, V, see Eq. (7). However, the re-sampling toward the lower losses is effectively not bound (i.e., formally it is bound at the zero loss, but the probability of a zero loss being re-sampled at F2–F3-rated wind speeds is albeit negligibly small). Therefore, the RDR method on average produces smaller losses and the discrepancy between the mean DR and RDR losses increases with tornado intensity (i.e., compare the second and third columns in Fig. 14). The losses, once again, scale linearly with the wind farm capacity.

4 Conclusions

Wind turbines are often exposed to adverse weather conditions, which sometimes include tornadoes of different intensities. Since Germany continues to lead the progress in wind power generation in Europe, this study investigated the damage and losses to wind turbines

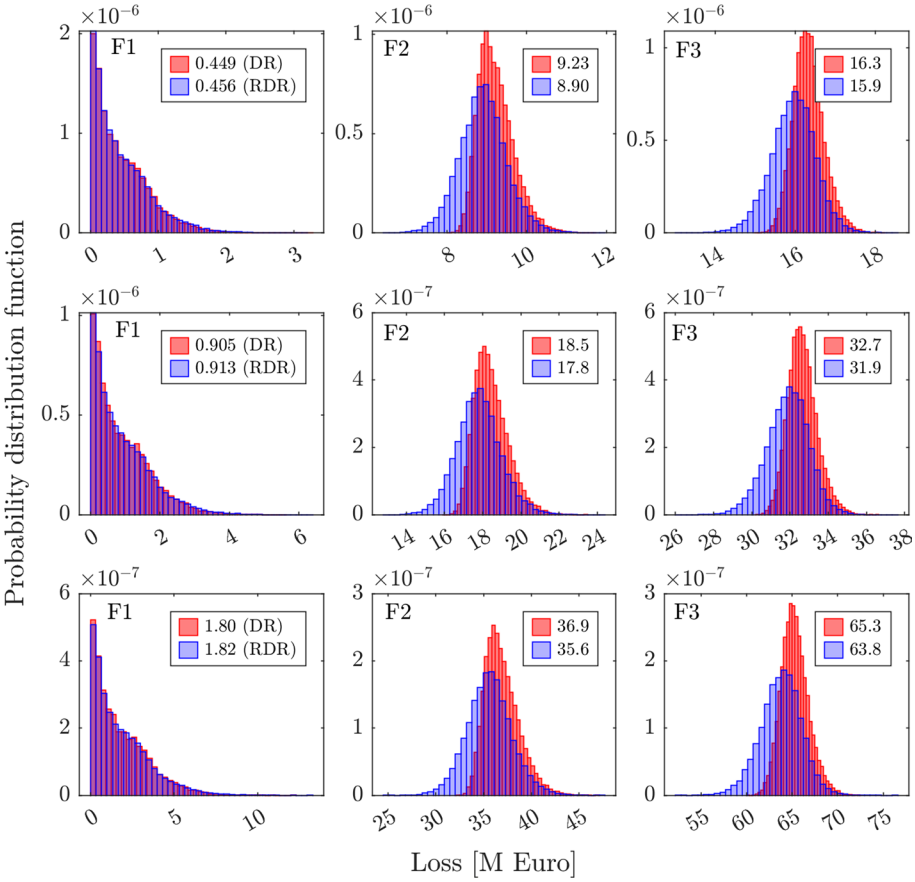

Fig. 14 Histograms of AGG losses caused by the single tornado track placed over a wind farm as indicated in Fig. 13. Columns correspond to different F scales (F1–F3) and rows correspond to wind turbines' capacities halved (first row), unchanged (second row) and doubled (third row). The mean values of the losses are shown in each plot for the DR (red) and RDR (blue) vulnerability modeling methods

caused by tornadoes across Germany. On average, Germany received 48 tornadoes per year in the period 1998–2021. It is logical to expect that a wind turbine-tornado interaction is a matter of time.

In this study, we proposed a hazard modeling approach by which Monte Carlo simulations were used to combine tornado climatology (the annual spatiotemporal occurrence of tornadoes per intensity, length, width, and orientation of tornado tracks), exposure map of wind turbines and their installed capacities, vulnerability curve, and financial module of wind turbine costs to estimate financial losses associated with tornado damage to wind turbines. The vulnerability function in the form of a generalized logistic curve was first proposed in this study. More precisely, the reported wind turbine damage in the form of categorical data—the so-called degrees of damage— was transformed into a continuous function using the generalized logistic curve. The annual number of tornadoes was represented using the negative binomial distribution, whereas their spatial frequency of occurrence across Germany was modeled by means of a kernel density estimator with normal

distribution in both longitudinal and latitudinal directions. Variations of tornadoes' path lengths and widths were simulated using a Weibull distribution and a log-normal distribution was used to represent the randomness of wind speeds across different tornado intensities. A kernel estimator was utilized to model the prevailing bearing angle of tornado tracks. These underlying distributions were based on the published literature. Lastly, we linked the financial cost (i.e., losses) of a damaged wind turbine as a percentage of the total cost of the unit by accounting for the costs of major wind turbine components. The results were presented in terms of the aggregated loss (AGG—sum of all losses in a year) and occurrence loss (OCC—the highest loss in a year) curves plotted as a function of the return period (RP). These probability exceedance curves are often used in the insurance sector and operational market to estimate the risk associated with a given peril (i.e., tornadoes).

Our statistical model properly replicated both temporal and spatial distributions of tornado occurrence across Germany. Over 65% of tornadoes were the weakest twisters (F0—based on the Fujita scale) and only about one-third of tornadoes had the potential to cause damage to wind turbines (F1 and stronger). Moreover, about 10% of tornadoes were severe (F2 and stronger). Weak tornadoes were more frequent in northwest Germany, whereas the stronger tornadoes were more common in the mid-west and east parts of the country. The highest occurrence of tornadoes was during the summer months, which is also the season characterized by low wind turbine capacity factors and somewhat lower electricity consumption than in the cold part of the year.

We used two approaches to simulate losses: (1) a deterministic relationship (DR) between damage and loss (i.e., deterministic vulnerability function); and (2) added randomness in the deterministic relationship (RDR) by allowing the damage to be normally distributed around the mean that was calculated using the DR approach. While the two methods produced similar losses for the high-frequency events (i.e., short return periods), the DR model gave more variability of the results in the low-frequency region (i.e., long return periods beyond ~500 years). The OCC losses for the DR approach were also larger than those for the RDR case in the tail region of the curves. We also demonstrated that doubling the number of current wind turbines (2NUM scenario) results in more minor losses than installing fewer but more powerful wind turbine units (2CAP scenario—the so-called repowering). We deemed this result as an important consideration for future planning of the wind energy sector in Germany.

We also investigated an idealized case in which a tornado track of a fixed length and width was repeatedly placed over the same wind farm that contained 17 wind turbines. The tornado intensity, wind turbine capacity and vulnerability function modeling (DR and RDR) were varied in order to quantify the sensitivity of our model to these parameters. While the losses caused by F1 tornadoes were practically independent of the vulnerability treatment, a significant distinction between DR and RDR was observed for F2 and F3 tornadoes. In all cases, the loss and capacity were linearly correlated. The probability of a tornado of different intensities hitting a wind turbine in Germany was also calculated.

Acknowledgements We acknowledge the support of the Natural Sciences and Engineering Research Council of Canada (NSERC) Science Undergraduate Research Award (SURA). The authors thank Dr. Tanya Brown-Giammanco from Texas Tech University (TTU) and the National Institute of Standards and Technology (NIST) for providing us with the tornado damage data that are used to formulate the vulnerability curve in this study. Our special thank goes to Dan Parvu for his help in obtaining the exposure map and MATLAB coding. We thank Dr. Ebba Dellwik and Kenneth Thomsen from Risø DTU for their help in estimating wind turbine costs. We express our gratitude to the European Severe Weather Database (ESWD; https://www.eswd.eu/), in particular Thomas Schreiner, for supplying us with the tornado database that was used in our study.

Funding Author Romane Bouchard has received funding from the Natural Sciences and Engineering Research Council of Canada (NSERC) Undergraduate Student Research Awards (USRA) 2022.

Data availability Data will be made available on request.

Code availability Code will be made available on request.

Declarations

Conflict of interest The authors declare that they have no known competing financial interests or personal relationships that could have appeared to influence the work reported in this paper.

Ethical approval The study followed the accepted principles of ethical and professional conduct throughout the research work. No animals or human participants are involved in this research.

References

Allen JT, Karoly DJ, Walsh KJ (2014) Future Australian severe thunderstorm environments part i: a novel evaluation and climatology of convective parameters from two climate models for the late twentieth century. J Clim 27(10):3827–3847. https://doi.org/10.1175/JCLI-D-13-00425.1

Arnold U, Özgür Yildiz (2015) Economic risk analysis of decentralized renewable energy infrastructures–a Monte Carlo simulation approach. Renew Energy 77:227–239. https://doi.org/10.1016/j.renene.2014.11.059

Bach PF (2022) International time series 2006-18. http://www.pfbach.dk/

Blanco MI (2009) The economics of wind energy. Renew Sust Energ Rev 13(6):1372–1382. https://doi.org/10.1016/j.rser.2008.09.004

Brooks HE (2004) On the relationship of tornado path length and width to intensity. Wea Forecasting 19(2):310. https://doi.org/10.1175/1520-0434(2004)019<0310:OTROTP>2.0.CO;2

Brooks HE, Lee JW, Craven JP (2003) The spatial distribution of severe thunderstorm and tornado environments from global reanalysis data. Atmos Res 67–68:73–94. https://doi.org/10.1016/S0169-8095(03)00045-0. (**european Conference on Severe Storms 2002**)

Daneshvaran S, Morden RE (2007) Tornado risk analysis in the United States. J Risk Finance 8:97–111. https://doi.org/10.1108/15265940710732314

Dessens J, Snow JT (1993) Comparative description of tornadoes in France and the United States. Am Geophys Union (AGU) 79:427–434. https://doi.org/10.1029/GM079p0427

Diffenbaugh NS, Scherer M, Trapp RJ (2013) Robust increases in severe thunderstorm environments in response to greenhouse forcing. Proc Natl Acad Sci USA 110(41):16,361-16,366. https://doi.org/10.1073/pnas.1307758110

Dotzek N (2001) Tornadoes in Germany. Atmos Res 56(1):233–251. https://doi.org/10.1016/S0169-8095(00)00075-2

Dotzek N, Grieser J, Brooks HE (2003) Statistical modeling of tornado intensity distributions. Atmos Res 67–68:163–187. https://doi.org/10.1016/S0169-8095(03)00050-4. (**european Conference on Severe Storms 2002**)

Dotzek N, Groenemeijer P, Feuerstein B et al (2009) Overview of essl's severe convective storms research using the European severe weather database eswd. Atmos Res 93(1):575–586. https://doi.org/10.1016/j.atmosres.2008.10.020. (**4th European Conference on Severe Storms**)

Edwards R, LaDue JG, Ferree JT et al (2013) Tornado intensity estimation: past, present, and future. Bull Amer Meteorol Soc 94(5):641–653. https://doi.org/10.1175/BAMS-D-11-00006.1

Eichhorn M, Scheftelowitz M, Reichmuth M et al (2019) Spatial distribution of wind turbines, photovoltaic field systems, bioenergy, and river hydro power plants in Germany. Data. https://doi.org/10.3390/data4010029

Elsner JB, Michaels LE, Scheitlin KN et al (2013) The decreasing population bias in tornado reports across the central plains. Weather Clim Soc 5(3):221–232. https://doi.org/10.1175/WCAS-D-12-00040.1

Elsner JB, Jagger TH, Elsner IJ (2014) Tornado intensity estimated from damage path dimensions. PLoS One 9(9):1–7. https://doi.org/10.1371/journal.pone.0107571

ESWD (2022) European severe weather database. https://eswd.eu/cgi-bin/eswd.cgi

Fan F, Pang W (2019) Stochastic track model for tornado risk assessment in the US. Front Built Environ. https://doi.org/10.3389/fbuil.2019.00037
Fujita TT (1971) Proposed characterization of tornadoes and hurricanes by area and intensity. Research Paper SMRP Research Paper No. 91, University of Chicago, Department of the Geophysical Sciences, Chicago, Illinois, United States. http://archive.org/details/nasa_techdoc_19720008829
Germer S, Kleidon A (2019) Have wind turbines in Germany generated electricity as would be expected from the prevailing wind conditions in 2000–2014? PLoS One 14(2):1–16. https://doi.org/10.1371/journal.pone.0211028
Ghosh A, Rafkin S (2012) Review of methods for estimation of high wind and tornado hazard frequencies. https://www.nrc.gov/docs/ML1930/ML19305C919.pdf
Groenemeijer P, Kühne T (2014) A climatology of tornadoes in Europe: results from the European severe weather database. Mon Weather Rev. https://doi.org/10.1175/MWR-D-14-00107.1
GTAI (2022) Germany trade and invest (gtai): Germany's wind energy industry- opportunities in a sustainable business environment. https://www.gtai.de/en/invest/industries/energy/wind-energy#76822
Hagen M, Finke U (1999) Motion characteristics of thunderstorms in southern Germany. Meteorol Appl 6(3):227–239. https://doi.org/10.1017/S1350482799001164
IEA (2017) World energy outlook 2017. https://www.iea.org/reports/world-energy-outlook-2017
IEA (2021) World energy outlook 2021. https://www.iea.org/reports/world-energy-outlook-2021
IRENA (2019) Future of wind deployment, investment, technology, grid integration and socio-economic aspects. https://www.irena.org/-/media/files/irena/agency/publication/2019/oct/irena_future_of_wind_2019.pdf
Justus CG, Hargraves WR, Yalcin A (1976) Nationwide assessment of potential output from wind-powered generators. J Appl Meteorol 15(7):673–678. https://doi.org/10.1175/1520-0450(1976)015<0673:NAOPOF>2.0.CO;2
Lepore C, Abernathey R, Henderson N et al (2021) Future global convective environments in cmip6 models. Earth's Future. https://doi.org/10.1029/2021EF002277
Marshall P, Brown-Giammanco T, Krautwurst N (2022) The current revision of the enhanced fujita (ef) scale. In: The 14th Americas conference on wind engineering (ACWE2022)
Martin-Tretton M, Reha M, Drunsic M, et al (2012) Data collection for current u.s. wind energy projects: component costs, financing, operations, and maintenance. https://www.nrel.gov/docs/fy12osti/52707.pdf
Maruf MNI (2021) Open model-based analysis of a 100% renewable and sector-coupled energy system-the case of Germany in 2050. Appl Energy 288(116):618. https://doi.org/10.1016/j.apenergy.2021.116618
McDonald JR, Mehta KC, Mani S (2006) A Recommendation for an Enhanced Fujita Scale (EF-Scale). Tech. Rep. revision 2, Wind science and engineering center, Texas Tech University, Lubbock, Texas, http://www.spc.noaa.gov/efscale/ef-ttu.pdf
Meyer CL, Brooks H, Kay MP (2002) A hazard model for tornado occurrence in the united states. In: Climate variations and forecasting (joint with the 16th conference probability and statistics and the 13th symposium on global change and climate variations). American Meteorological Society, Orlando, Florida, USA
Papathoma-Köhle M, Keiler M, Totschnig R et al (2012) Improvement of vulnerability curves using data from extreme events: a debris flow event in south tyrol. Nat Hazards 64:2083–2105. https://doi.org/10.1007/s11069-012-0105-9
Refan M, Romanic D, Parvu D et al (2020) Tornado loss model of Oklahoma and Kansas, United States, based on the historical tornado data and Monte Carlo simulation. Int J Disaster Risk Reduct 43(101):369. https://doi.org/10.1016/j.ijdrr.2019.101369
Romanic D, Refan M, Wu CH et al (2016) Oklahoma tornado risk and variability: a statistical model. Int J Disaster Risk Reduct 16:19–32. https://doi.org/10.1016/j.ijdrr.2016.01.011
Romanic D, Parvu D, Refan M et al (2018) Wind and tornado climatologies and wind resource modelling for a modern development situated in "tornado alley''. Renew Energy 115:97–112. https://doi.org/10.1016/j.renene.2017.08.026
Romanic D, Chowdhury J, Chowdhury J et al (2020) Investigation of the transient nature of thunderstorm winds from Europe, the United States, and Australia using a new method for detection of changepoints in wind speed records. Mon Weather Rev 148(9):3747–3771. https://doi.org/10.1175/MWR-D-19-0312.1
Romanic D, Taszarek M, Brooks H (2022) Convective environments leading to microburst, macroburst and downburst events across the united states. Weather Clim Extrem. https://doi.org/10.1016/j.wace.2022.100474
Salameh JP, Cauet S, Etien E et al (2018) Gearbox condition monitoring in wind turbines: a review. Mech Syst Signal Process 111:251–264. https://doi.org/10.1016/j.ymssp.2018.03.052

Sarajcev P, Vasilj J, Goic R (2013) Monte Carlo analysis of wind farm surge arresters risk of failure due to lightning surges. Renew Energy 57:626–634. https://doi.org/10.1016/j.renene.2013.03.004
Schaefer JT, Kelly DL, Abbey RF (1986) A minimum assumption tornado-hazard probability model. J Appl Meteorol Climatol 25(12):1934–1945. https://doi.org/10.1175/1520-0450(1986)025<1934:AMATHP>2.0.CO;2
Seeley JT, Romps DM (2015) The effect of global warming on severe thunderstorms in the united states. J Clim 28(6):2443–2458. https://doi.org/10.1175/JCLI-D-14-00382.1
Seguro J, Lambert T (2000) Modern estimation of the parameters of the weibull wind speed distribution for wind energy analysis. J Wind Eng Ind Aerodyn 85(1):75–84. https://doi.org/10.1016/S0167-6105(99)00122-1
Standohar-Alfano C, Lindt J (2015) Empirically based probabilistic tornado hazard analysis of the united states using 1973–2011 data. Nat Hazards Rev 16(04014):013. https://doi.org/10.1061/(ASCE)NH.1527-6996.0000138
Strader S, Walker A, Pingel T et al (2017) Projected 21st century changes in tornado exposure, risk, and disaster potential. Clim Change. https://doi.org/10.1007/s10584-017-1905-4
Strader SM, Pingel TJ, Ashley WS (2016) A monte carlo model for estimating tornado impacts. Meteorol Appl 23(2):269–281. https://doi.org/10.1002/met.1552
Thom HCS (1963) Tornado probabilities. Mon Weather Rev 91(10):730–736. https://doi.org/10.1175/1520-0493(1963)091<0730:TP>2.3.CO;2
Tippett MK, Allen JT, Gensini VA et al (2015) Climate and hazardous convective weather. Curr Clim Change Rep 1:60–73. https://doi.org/10.1007/s40641-015-0006-6
Totschnig R, Fuchs S (2013) Mountain torrents: quantifying vulnerability and assessing uncertainties. Eng Geol 155:31–44. https://doi.org/10.1016/j.enggeo.2012.12.019
Totschnig R, Sedlacek W, Fuchs S (2011) A quantitative vulnerability function for fluvial sediment transport. Nat Hazards 58:681–703. https://doi.org/10.1007/s11069-010-9623-5
UFZ (2019) Geocoded asset master data of on-shore wind power, photovoltaic field systems, bioenergy and river hydro power plants in germany until 2015. https://doi.org/10.48758/UFZ.5467. Accessed on 30 April 2022
Walker GR (2011) Modelling the vulnerability of buildings to wind. Can J Civ Eng 38(9):1031–1039. https://doi.org/10.1139/l11-047
WISDEM (2019) The wind-plant integrated system design and engineering model. https://wisdem.readthedocs.io/en/master/index.html